Detecting alkali-silica reaction in thick concrete structures using linear array ultrasound

N. Dianne Bull Ezell[*a], Austin Albright[a], Dwight Clayton[a], Hector Santos-Villalobos[a]
[a]Oak Ridge National Laboratory, 1 Bethel Valley Rd, Oak Ridge, TN 37830

ABSTRACT

Commercial nuclear power plants (NPPs) depend heavily on concrete structures—making the long-term performance of these structures crucial for safe operation, especially with license period extensions to 60 years and possibly beyond. Alkali-silica reaction (ASR) is a reaction that occurs over time in concrete between alkaline cement paste and reactive, noncrystalline silica (aggregates). In the presence of water, an expansive gel is formed within the aggregates, which results in microcracks in aggregates and adjacent cement paste. ASR can potentially affect concrete properties and performance characteristics such as compressive strength, modulus of elasticity, flexural stiffness, shear strength, and tensile strength. Currently, no nondestructive evaluation methods have proven effective in identifying ASR before surface cracks form. ASR is identified visibly or by petrographic analysis. Although ASR definitely impacts concrete material properties, the performance of concrete structures exhibiting ASR depends on whether or not the concrete is unconfined or confined with reinforcing bars. Confinement by reinforcing bars restrains the expansion of ASR-affected concrete, similar to prestressing, thus improving the performance of a structure. Additionally, there is no direct correlation between the mechanical properties of concrete sample cores and the in-situ properties of the concrete. The University of Tennessee–Knoxville, Oak Ridge National Laboratory, and a consortium of universities have developed an accelerated ASR experiment. Three large concrete specimens, representative of NPP infrastructure, were constructed containing both embedded and surface instruments. This paper presents preliminary analysis of these specimens using a frequency-banded synthetic aperture focusing technique.

Keywords: Nondestructive evaluation, alkali-silica reaction, frequency-banded synthetic aperture focusing technique

1. INTRODUCTION

The US Department of Energy (DOE) is interested in developing solutions to improve reliability, sustain the safety, and extend the operating lifetimes of nuclear power plants (NPPs) beyond 60 years. Research programs studying the degradation of structural materials such as concrete are critical because so many safety structures are composed of concrete [1]. The research presented here is funded by the DOE Light Water Reactor Sustainability Program to study the effects of alkali-silica reaction (ASR) expansion within large concrete structures. This paper discusses three large specimens designed and constructed at the University of Tennessee–Knoxville (UTK), the nondestructive evaluation (NDE) of these specimens, and the preliminary analysis of the collected data.

1.1 ASR Concrete Specimens

The three large UTK concrete specimens are 3 m × 3.5 m × 1 m [2], making them some of the largest test specimens currently available for evaluating ASR development (see Figure 1). The University of Alabama developed two concrete mixtures: the first ensures ASR development, and the second is a control mixture. Dr. Eric Giannini created a reactive mixture with coarse aggregate and added NaOH to expedite the reaction between the aggregate and paste. The two specimens containing this mixture are referred to as the UASR (for unconfined ASR) and CASR (for confined ASR) specimens. The control mixture uses the same aggregates with $LiNO_3$ to eliminate swelling of the ASR gel. The specimen with this mixture is referred to as CTRL. All three specimens have two mats of #11 rebar spaced at 25 cm on center [1]. The specimens are designed to replicate expansion (reactive mixture) under two conditions: confined and unconfined expansion. To make the experiment representative of conditions expected at a

NPP, such as passive restraint, the confined (CASR) specimen was poured inside a steal frame (see Figure 2). The frame allows expansion in the z axis only and prevents lateral expansion.

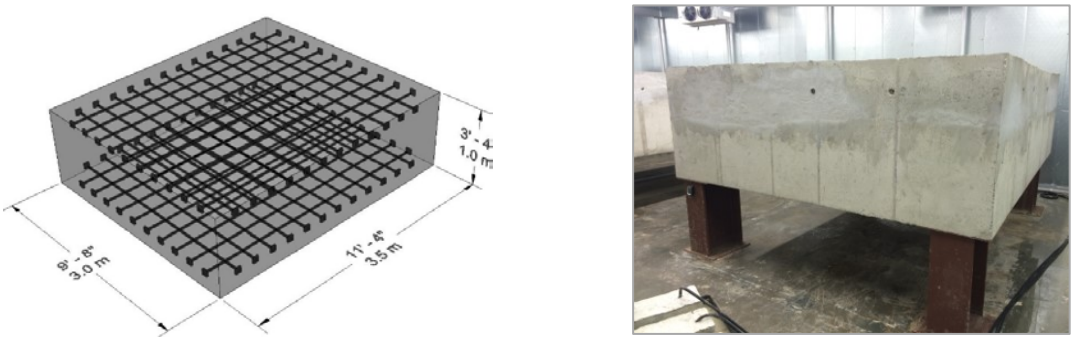

(a) (b)

Figure 1. (a) Unconfined concrete specimen design drawing. (b) One of the finished unconfined concrete specimens, poured on July 23, 2016.

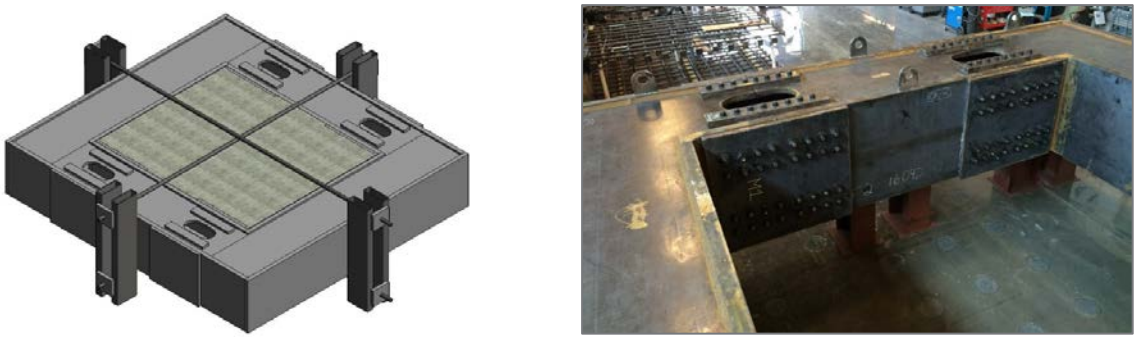

(a) (b)

Figure 2. (a) Confined concrete specimen design drawing. (b) Steel frame built for the confined-ASR specimen.

The specimens were constructed inside an environmental chamber to control humidity and temperature. The concrete mix was designed to expand 0.5% over a two-year period. The chamber originally maintained a 100°F temperature with 95% relative humidity (see Figure 3). However, after the first year of the experiment, the expansion was accelerating at a much faster rate. Results from several collaborators predicted that expansion would be completed before the two-year target; therefore, the temperature was reduced to 75°F with 95% humidity on July 28, 2017 [3]. The chamber has since stabilized to a temperature of 88°F.

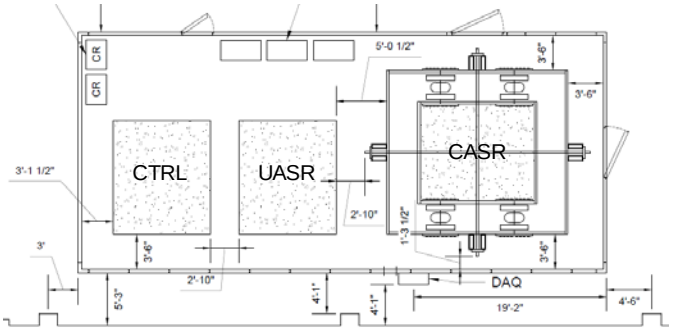

Figure 3. Engineering drawing of the environmental chamber built around the concrete specimen to maintain the desired temperature and humidity.

NDE of these specimens was performed on two separate occasions by the University of Minnesota in collaboration with the University of Pittsburg. The first evaluation occurred on January 20, 2017. The second evaluation occurred on September 29, 2017. The measurement procedure and preliminary results are discussed in the next section.

1.2 NDE Instrumentation

A commercial ultrasonic tomography unit, MIRA, by Germann Instruments, Inc, consisting of a linear array of dry point contact (DPC) transducers (see Figure 4) was used for the NDE data collection. The DPC transducers do not require a liquid coupling agent for the shear waves to penetrate the test medium correctly. This allows for quick transitions between test locations, shortening the overall measurement time. The linear array is multifunctional and operates by transmitting an ultrasonic pulse from one column of DPC contacts, while receiving on the DPC contacts of the other nine columns (see Figure 4b). Each column of DPC transducers is treated as a single entity internally by MIRA, so as the transmitting column of DPCs is cycled through all 10 columns, the other columns of DPCs receive a total of 45 unique impulse time-history measurements resulting from each "triggering" of the system. Each transducer column is spaced 40 mm (1.6 in.) apart, on center. The 45 unique measurement sequences collected result in the following sets of fixed horizontal spacing between the transmitting and receiving column of DPCs: nine unique pairings with 40 mm (1.6 in.) spacing, eight unique pairings with 80 mm (3.1 in.) spacing, seven unique parings with 120 mm (4.7 in.) spacing, six unique pairings with 160 mm (6.3 in.) spacing, etc., down to one unique pairing with 360 mm (14.2 in.) spacing [4]. Because these fixed spacings are part of the instrument itself, each of the 45 channels of data collected from MIRA can have the synthetic aperture focusing technique (SAFT) applied to it. Additionally, since the spacings and synchronization of 45 channels is fixed, the results of all 45 single channel SAFT reconstructions can be integrated into a single SAFT reconstruction, allowing all the information captured by each "firing" of the MIRA unit to be fused into a single cohesive SAFT reconstruction image.

The following procedure was followed for both NDE measurements in January 2017 and September 2017. The MIRA system parameters were set to operation center frequency = 50 kHz, impulse duration = 2 half-periods, and one cycle [3]. These parameters have been proven optimal for thick concrete NDE.

(a) (b)

Figure 4. (a) MIRA version 1 system. (b) MIRA version 1 ultrasonic array face. (Images courtesy of Germann Instruments, Inc.).

Measurements were collected from the top surface of all three concrete specimens (CTRL, UASR, and CASR). A 10 × 10 grid, with one axis labeled A-J and the perpendicular axis of the grid labeled 1-10, was drawn on the top face of each specimen (see Figure 5). Each of the parallel lines is 4 in. apart. Figure 5a shows the MIRA positioned for the first measurement at grid location (A, 1). The horizontal centerline of the MIRA instrument is aligned on line A, with the first large mark on the device aligned with line 1 (see red arrow). After the first measurement was completed, the MIRA instrument was moved along line A to each of the remaining grid lines, 2 through 9, and measurements were collected. The complete sweep along line A acquires 9 measurements, each containing 45 channels of data. This same sweep was repeated along lines B through J. After completing all 10 sweeps of the A-J lines, the MIRA was rotated perpendicular to the A-J lines and measurements were collected sweeping along each of lines 1 through 10. This same measurement process was repeated on the top face of all three specimens.

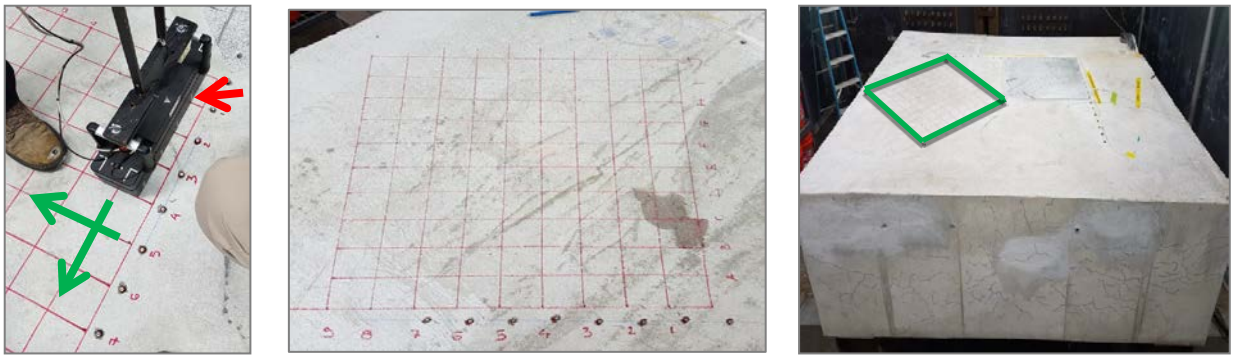

(a) (b) (c)

Figure 5. (a) A,1 location measurement with MIRA instrument. (b) Top surface of CTRL. (c) Top surface of UASR [3].

Measurements were collected using MIRA from the side face of the two unconfined specimens (CTRL and UASR). A similar positioning grid was used, with one axis of the grid labeled A–E and the perpendicular axis of the grid labeled 1–5. A lateral measurement sweep along line A is illustrated on the right side of Figure 6. A horizontal measurement sweep of line 1 is illustrated at the bottom of Figure 6.

Figure 6. Lateral surface grid with lateral MIRA measurements on line A and horizontal MIRA measurements on line 1.

The results from these measurements were reconstructed using a frequency-banded SAFT implementation [5]. This technique is a modified version of existing SAFT algorithms.

2. FREQUENCY-BANDED SAFT

SAFT [6, 7, 8] is a commonly used method for reconstruction of time-of-flight signals, such as ultrasound. SAFT is a delay and sum technique that requires a time of flight of each ultrasonic echo along with the speed of sound in the material to function properly [3]. The reconstruction result is a "B-scan" or cross-sectional image of the interior of the concrete specimen [9]. Frequency-banded SAFT augments the typical SAFT workflow by segmenting the time-series data into different frequency bands using wavelets immediately before performing the SAFT reconstructions [5]. This allows suppression of artifacts and background noise through the removal of specific bands of frequency content, that is, the energy contained in specific frequency bands. The frequency-banded data is then returned to the time domain but with only the energy of the desired frequency bands retained. The frequency-banded time domain data is then supplied as the input to SAFT. Frequency-banded SAFT does have a limitation though; as the frequency content\energy is reduced, the sharpness of the boundary at a reflective object might also decrease. This decrease is related to the reduction in energy as the retained frequency bands become narrower and fewer. More simply put, there is a point at which too few frequencies, and thus too little energy, are retained and the reflecting object might be quite blurred. However, a counterpoint to this potential issue is that frequency banding also allows frequency-dependent characteristics such as shifts in frequency caused by a defect that needs to be investigated and noise that needs to be removed.

The effectiveness of frequency-banded SAFT was validated on specimens with known ASR at the Electric Power Research Institute's (EPRI's) Charlotte, North Carolina, location [9]. The SAFT reconstructions display a clear difference between the specimens with ASR and the ones without (see Figure 7). The dark blue region at the top of the images is the top face of the specimen, and the dark red regions are the back wall reflection. The specimen impacted by ASR in Figure 7b shows an increase in reflections in the region between the back wall and top surface caused by multiple ASR scatters inside the concrete [9].

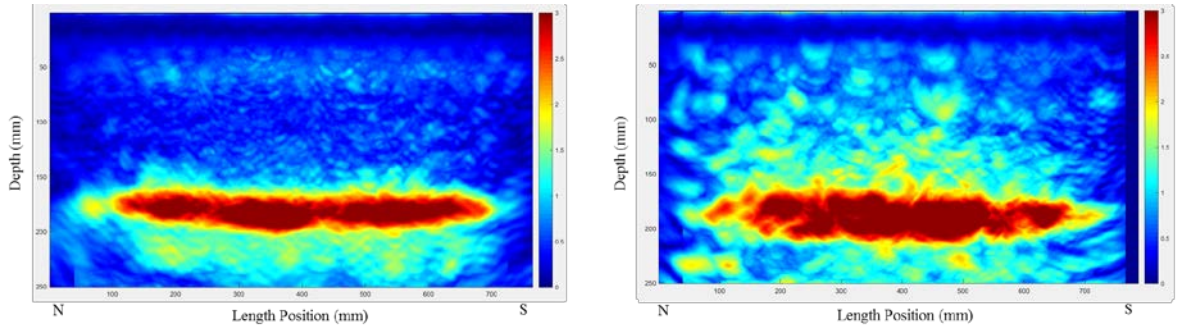

(a) (b)

Figure 7. (a) SAFT reconstruction of the EPRI concrete specimen without ASR. (b) SAFT reconstruction of the EPRI concrete specimen with known ASR defects.

This same analysis technique was used for reconstruction of the data obtained from the UTK thick concrete specimens. The SAFT B-scan reconstructions were used to build panoramic B-scan images of the acquired data along an entire positioning grid line (e.g., line-A). They show the internal characteristics across the entire cross-section of the grid line [10] (see Figure 8). The grid lines labeled with letters correspond to horizontal reconstructions, and the grid lines labeled with numbers correspond to vertical reconstructions. The color code in these reconstructions is the same as the code in Figure 7. The intensity of a pixel is proportional to the intensities of the sound waves reflected at that point. The yellow and red, bright pixels, in Figure 8, correspond to the rebar mats of #11 rebar. The ultrasound signals are reflected when there is a change in the mediums acoustic impedance.

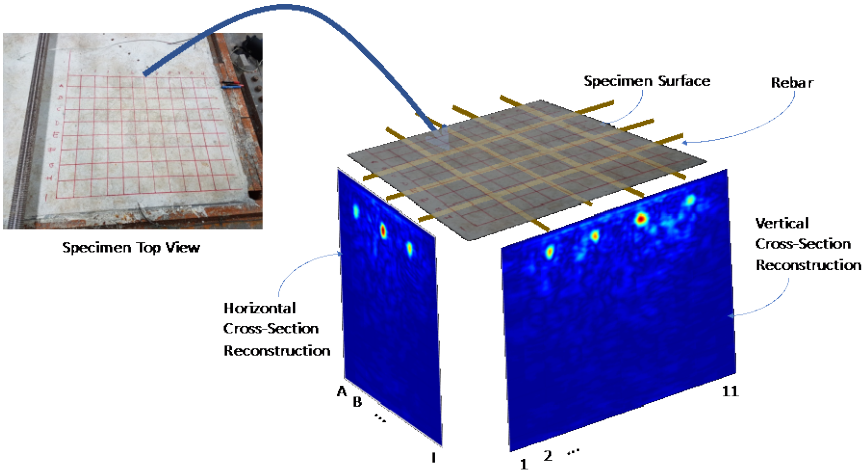

Figure 8. Reconstruction example of top surface NDR measurement of confined specimen (CASR) [3].

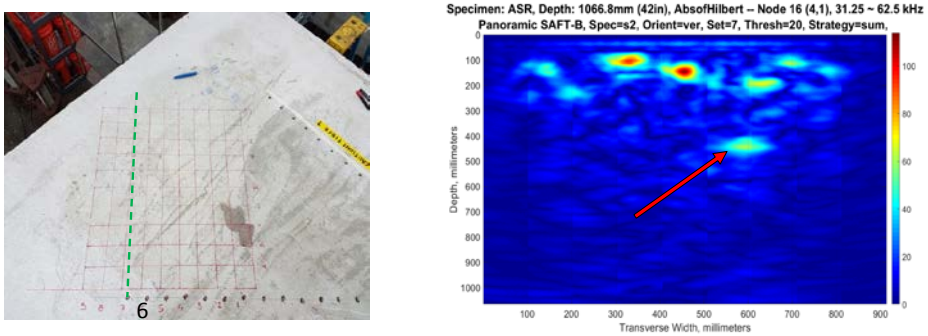

(a) (b)

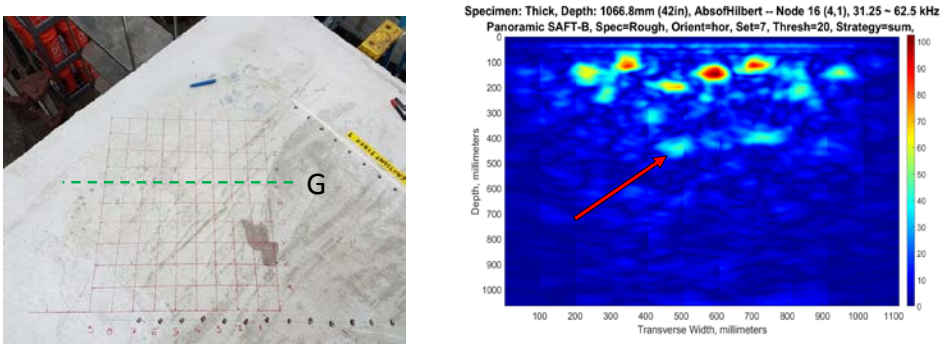

(c) (d)

Figure 9. (a) UASR grid line 6. (b) SAFT vertical reconstruction UASR grid line 6. (c) UASR grid line G. (b) SAFT horizontal reconstruction UASR grid line G.

The preliminary analysis of the UASR specimen shows high amounts of reflectivity, which would be indicative of developing ASR (see Figure 9). The red arrow in Figure 9b and Figure 9d points to what could be localized ASR growth. Futher verification with other collaborators will determine if this location actually has localized ASR.

3. CONCLUSIONS

This document discusses ongoing research and development of NDE techniques developed for ASR detection. Three thick concrete specimens designed and constructed to be representative of the concrete structures within NPPs were analyzed. ASR is known to cause structural issues by affecting concrete properties and performance characteristics such as compressive strength, modulus of elasticity, flexural stiffness, shear strength, and tensile strength. Frequency-banded SAFT was applied to the ultrasonic data collected using a commercially available MIRA instrument for NDE of concrete specimens. The MIRA instrument and frequency-banded SAFT algorithm were evaluated on known ASR specimens at the EPRI Charlotte location and proved suitable for this application. The frequency-banded SAFT identified regions with ASR in the EPRI Charlotte specimens. The system was then employed to make NDE measurements on thick concrete specimens built at UTK. Verification from other collaborators is needed, but likely locations of ASR development were identified using MIRA and frequency-banded SAFT.

REFERENCES

[1] Ezell, N. D. B, Hayes, N., Lenarduzzi, R., Clayton, D., Ma, Z., Le Pape, S. and Le Pape, Y., "Experimental Collaboration for Thick Concrete Structures with Alkali-Silica Reaction," Proc. QNDE, 2017.

[2] University of Tennessee, "Concrete Testing for Nuclear Application," 22 September 2016, http://cee.utk.edu/new-video-explains-ut-and-ornl-research-on-concrete-for-nuclear-application (25 August 2017).

[3] Ezell, N. D. B., Santos-Villalobos, H., Clayton, D., Floyd, D. and Khazanovich, L., *Linear Array Ultrasonic Testing for the Detection of Alkali-Silica Reaction in Thick Concrete Specimens*, ORNL/TM-2017/393, Oak Ridge National Laboratory, August 2017.

[4] Hoegh, K. and Khazanovich L., "Correlation Analysis of 2D Tomographic Images for Flaw Detection in Pavements," Journal of Testing and Evaluation. American Society for Testing and Materials 40(2), 247-255 (2012).

[5] Albright, A. and Clayton, D., "The benefits of using time-frequency analysis with synthetic aperture focusing technique," Proc. AIP Conference, 1650(1), 94-103, (2015).

[6] Shao, Z., Shi, L. and Cai, J., Rev. Sci. Instrum. Review of Scientific Instruments 82, 073708 (2011).

[7] Engle, B. J., Schmerr, J. L. W. and Sedov, A., Proc. AIP Conference, 1581, 49 (2014).

[8] Dobie, G., Pierce, S. G. and Hayward, G., NDT and E International 58, 10-17 (2013).

[9] Clayton, Dwight A., Santos-Villalobos, H., Ezell, N. D. B., Clayton, J. and Baba, J., "Automated Detection of Alkali-Silica Reaction in Concrete Using Linear Array Ultrasound Data," [Environmental Degradation of Materials in Nuclear Power Systems*]* Springer, Cham, (2017).

[10] Clayton, D. A., Hoegh, K. and Khazanovich, L., *Thick Concrete Specimen Construction, Testing, and Preliminary Analysis*, ORNL/TM-2015/72, Oak Ridge National Laboratory, March 2015.